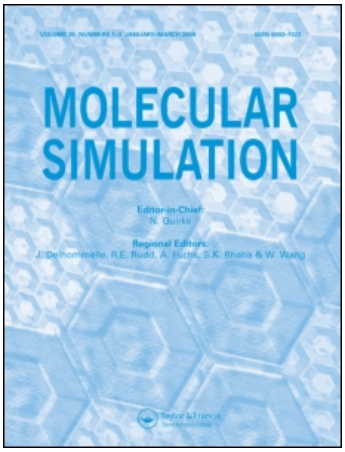

Molecular Simulation
Publication details, including instructions for authors and subscription information:
http://www.informaworld.com/smpp/title~content=t713644482

Molecular dynamics simulations to investigate the relationship between the structural stability and amyloidogenesis of the wild-type and N-terminal hexapeptide deletion ΔN6 β2-microglobulin

Po-Sheng Fang[a]; Jian-Hua Zhao[b]; Hsuan-Liang Liu[ab]; Kung-Tien Liu[c]; Jenn-Tzong Chen[d]; Wei-Bor Tsai[e]; Hsin-Yi Lin[a]; Hsu-Wei Fang[b]; Yih Ho[f]
[a] Graduate Institute of Biotechnology, National Taipei University of Technology, Taipei, Taiwan, ROC [b] Department of Chemical Engineering and Biotechnology, National Taipei University of Technology, Taipei, Taiwan, ROC [c] Chemical Analysis Division, Institute of Nuclear Energy Research, Taiwan, ROC [d] Isotope Application Division, Institute of Nuclear Energy Research, Taiwan, ROC [e] Department of Chemical Engineering, National Taiwan University, Taipei, Taiwan, ROC [f] School of Pharmacy, Taipei Medical University, Taipei, Taiwan, ROC

To cite this Article Fang, Po-Sheng , Zhao, Jian-Hua , Liu, Hsuan-Liang , Liu, Kung-Tien , Chen, Jenn-Tzong , Tsai, Wei-Bor , Lin, Hsin-Yi , Fang, Hsu-Wei and Ho, Yih(2009) 'Molecular dynamics simulations to investigate the relationship between the structural stability and amyloidogenesis of the wild-type and N-terminal hexapeptide deletion ΔN6 β2-microglobulin', Molecular Simulation, 35: 9, 755 — 765
To link to this Article: DOI: 10.1080/08927020902818005
URL: http://dx.doi.org/10.1080/08927020902818005

Molecular Simulation
Vol. 35, No. 9, August 2009, 755–765

Taylor & Francis
Taylor & Francis Group

Molecular dynamics simulations to investigate the relationship between the structural stability and amyloidogenesis of the wild-type and N-terminal hexapeptide deletion ΔN6 β2-microglobulin

Po-Sheng Fang[a], Jian-Hua Zhao[b], Hsuan-Liang Liu[ab]*, Kung-Tien Liu[c], Jenn-Tzong Chen[d], Wei-Bor Tsai[e], Hsin-Yi Lin[a], Hsu-Wei Fang[b] and Yih Ho[f]

[a]*Graduate Institute of Biotechnology, National Taipei University of Technology, 1 Section 3, ZhongXiao East Road, Taipei 10608, Taiwan, ROC;* [b]*Department of Chemical Engineering and Biotechnology, National Taipei University of Technology, 1 Section 3, ZhongXiao East Road, Taipei 10608, Taiwan, ROC;* [c]*Chemical Analysis Division, Institute of Nuclear Energy Research, 1000, Wunhua Road, Longtan Township, Taoyuan County 32546, Taiwan, ROC;* [d]*Isotope Application Division, Institute of Nuclear Energy Research, 1000, Wunhua Road, Longtan Township, Taoyuan County 32546, Taiwan, ROC;* [e]*Department of Chemical Engineering, National Taiwan University, 1 Section 4, Roosevelt Road, Taipei 106, Taiwan, ROC;* [f]*School of Pharmacy, Taipei Medical University, 250 Wu-Hsing Street, Taipei 110, Taiwan, ROC*

(*Received 30 July 2008; final version received 5 February 2009*)

β2-Microglobulin (β2m) forms amyloid fibrils in patients undergoing long-term haemodialysis, leading to dialysis-related amyloidosis. Proteolysis of the N-terminal region of β2m results in a truncation of the six N-terminal residues (ΔN6 β2m) in ~30% of the β2m molecules extracted from *ex vivo* fibrils. The ΔN6 β2m has been shown to exhibit a higher tendency for self-association comparing to the wild-type (wt) β2m, particularly at neutral pH. In order to gain atomic insights into the early stages of amyloid formation of the wt and ΔN6 β2m, various molecular dynamics simulations were conducted to investigate the stability and dynamics of these two molecules at various temperatures and neutral pH in this study. Our results, in agreement with previous experimental results, indicate that the structural stability of the ΔN6 β2m is lower than that of the wt β2m. It can be attributed to fact that the removal of the N-terminal six residues results in the loss of the salt–bridge interaction between residues R3 and D59, leading to the increased solvent exposure of the K3 peptide. It further allows water molecules to destabilise the interior region of the K3 peptide, leading to the elongation between the B- and E-strands. It may further accelerate the conformational changes of the ΔN6 β2m, leading to the formation of amyloid fibrils more readily at neutral pH. Our results also suggest that the K3 peptide may be a potential initiation site of amyloid formation for the ΔN6 β2m due to its increased solvent exposure. We further suggest that fibril morphology of the ΔN6 β2m formed at neutral pH is similar to that of the wt β2m formed at low pH (1.5–3) since they adopt the similar conformation with the elongation between B- and E-strands for their partially unfolded amyloidogenic intermediates.

Keywords: β2-microglobulin; dialysis-related amyloidosis; ΔN6 β2m; molecular dynamics simulations; K3 peptide; amyloidogenic intermediate

1. Introduction

More than 20 human diseases, including Alzheimer's disease, prion diseases, and dialysis-related amyloidosis (DRA), are associated with the pathological self-assembly of various soluble proteins into cytotoxic oligomers and amyloid fibrils [1–3]. Although these proteins share very little sequence identity and structural similarity in solution, the X-ray diffraction data show that all fibrils exhibit a common cross β-sheet structure with β-strands perpendicular and hydrogen bonds parallel to the fibril axis, suggesting a similar aggregation mechanism for all amyloidogenic proteins [4]. For DRA, the 99-residue human β2-microglobulin (β2m) [5], the light chain of the class I major histocompatibility complex (MHC-I), forms amyloid fibrils that deposit in the musculo-skeletal system in patients undergoing long-term haemodialysis [6]. After its release from the cells expressing MHC-I, β2m is carried to the kidney where it is degraded [7]. Patients with kidney dysfunction have a reduced ability to filter β2m from the plasma and consequently exhibit an up to 60-fold increase in the circulating level of β2m [6]. Through an undetermined mechanism, β2m forms amyloid fibrils that typically accumulate in the musculoskeletal system [8]. The wild-type (wt) β2m, belonging to the immunoglobin superfamily, adopts a seven-stranded β-sandwich fold [9,10]. The two β-sheets (one consisting of the A-, B-, D-, E-strands and the other consisting of the C-, F-, G-strands) are connected by a single disulphide bond between Cys25 and Cys80 from the B- and F-strands, respectively (Figure 1).

Both experimental and theoretical studies have been extensively performed to elucidate the amyloid formation of the wt β2m. The results of previous experimental studies have indicated that β2m forms two distinct fibril morphologies under acidic pH conditions. In the pH range of 3–5 in salt, the wt β2m forms short and curved fibrils;

*Corresponding author. Email: f10894@ntut.edu.tw

ISSN 0892-7022 print/ISSN 1029-0435 online

DOI: 10.1080/08927020902818005
http://www.informaworld.com

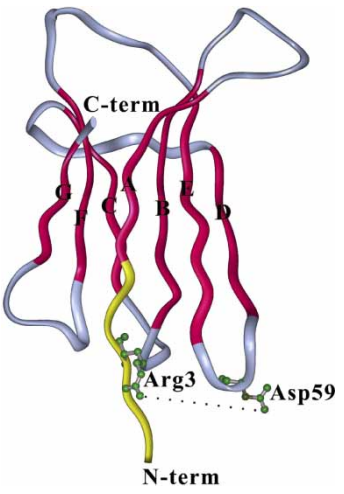

Figure 1. X-ray crystallographic structure of the wt β2m visualised by the Insight II program. Secondary structures are predicted according to DSSP (Kabsch and Sander, 1983); seven β-strands (A–G), red; The N- and C-termini are also indicated; truncation of the N-terminal six residues for ΔN6 β2m, yellow. The salt–bridge interaction between residues R3 and D59 in the wt β2m is shown in ball-and-stick. The K3 peptide (residues 20–41) corresponds to the B- and C-strands and the connecting B–C loop.

whereas in the pH range of 1.5–3 in salt, it forms long and straight fibrils [11–13]. These two distant fibril morphologies have been specifically related to two unfolded intermediates, I (I_1) and II (I_2) [11]. Computationally, Armen and Daggett [14] have determined the structures of the partially unfolded amyloidogenic intermediates (I_1 and I_2) of the wt β2m. Furthermore, previous theoretical study has revealed that the wt β2m forms domain-swapped dimer, in which the two monomers exchange their N-terminal segments complementing each other [15]. On the other hand, there is evidence that the 22-residue K3 peptide, Ser20–Lys41, obtained by the digestion of β2m with *Acromobacter* protease I, forms amyloid-like fibrils in various solutions [16,17]. These results suggest that the K3 peptide forms amyloid fibrils over a wide range of pH values with an optimum around pH 7 [17]. Previous study also showed that once the rigid native β2m is unfolded and additional factors triggering the nucleation process are provided, it readily forms amyloid fibrils at neutral pH [17]. The above experimental results imply that this minimal K3 peptide may be the initiation site for amyloid fibril formation of the full-length protein and may constitute the core of the resulting amyloid fibrils.

In addition, Bellotti et al. [18] have shown that proteolysis of the N-terminal region of the wt β2m results in a truncation of the six N-terminal residues (ΔN6 β2m) in ~30% of the β2m molecules extracted from *ex vivo* fibrils. The ΔN6 β2m was found to exhibit a higher tendency for self-association than the wt β2m. Unlike the wt β2m, the ΔN6 β2m is able to form amyloid fibrils at physiological pH condition [18–20]. Recently, Myers et al. [21] have shown that the ΔN6 β2m forms low yields of amyloid-like fibrils at pH 7.0 in the absence of seeds, suggesting that this species can initiate fibrillogenesis *in vivo*. Furthermore, previous data have shown that the addition of tiny amounts of the ΔN6 β2m to the wt β2m leads to the formation of large aggregates rapidly, suggesting a seeding capacity of this species in promoting β2m aggregation [22].

Understanding the dynamic behaviours of the amyloidogenic proteins is expected to provide insights into the possible mechanism of conformational change responsible for amyloid formation. Investigating the structural fluctuations of these proteins may provide knowledge for designing drugs to inhibit protein aggregation targeted at the flexible portion. To date, atomistic information for the aggregation of the ΔN6 β2m in explicit water is still limited. Usually, molecular dynamics (MD) simulations have four tactics to modify the physiological conditions: temperature [23–28], pressure [29], pH [25], or solvent [30]. Particularly, high-temperature (for example, 498 K) MD simulations have become a well-established tool to accelerate protein unfolding without changing the pathway of unfolding [31].

In order to investigate the atomistic details for the conformational change of the wt and ΔN6 β2m responsible for the early stages of amyloid formation, various MD simulations at different temperatures (310, 398, and 498 K) at neutral pH were conducted in this study. We aim to elucidate: (i) the structural stability and dynamics of the wt and ΔN6 β2m; (ii) the importance of the N-terminal six residues for the globular structural stability of β2m; (iii) the possible role of the K3 peptide for the unfolding of β2m; and (iv) the relationships between the fibril morphology and its related partially unfolded intermediate.

2. Methods

2.1 The construction of the wt and ΔN6 β2m model

Molecular minimisation and dynamics simulations were carried out using DISCOVER 2.9.8 of the Insight II molecular simulation software (Accelrys, San Diego, CA, USA) with the consistent valence force field [32]. The trajectories were analysed using ANALYSIS module of the Insight II program. All calculations were performed with NVT and periodic boundary conditions [33]. An atom-based distance cut-off was applied at 8 Å for both non-bonded electrostatic and van der Waals interactions. The X-ray crystallographic structure of the wt β2m was obtained from the Protein Data Bank (ID: 1lds) [10] and submitted to 5000 iterations with steepest gradient method, followed by 5000 iterations with conjugated gradient method. Six N-terminal residues of the wt β2m

were truncated to generate the ΔN6 β2m using the BIOPLYMER module of the Insight II program. The ΔN6 β2m was further refined by energy minimisation as for the wt β2m. The energy-minimised wt and ΔN6 β2m were separately placed in the centre of a rectangular box with the size of $60 \times 50 \times 50\,\text{Å}^3$ soaked with water molecules. To consider the effect of temperature in our simulation systems, solvent densities were adjusted by changing the numbers of solvent molecules in the box according to the experimental values of 0.993, 0.939, and 0.831 g/ml at 310, 398, and 498 K, respectively [34]. These systems were energy-minimised with the method described above until the maximum derivative was lower than $0.001\,\text{kcal mol}^{-1}\,\text{Å}^{-1}$. To further optimise the arrangement of the water molecules around the protein and alleviate high energy regions, water molecules alone were allowed to relax by running a short 150 ps MD simulation with position restraints applied to all the protein atoms at corresponding temperatures. Subsequently, protein alone was minimised with 5000 steps, followed by the minimisation of the entire system for additional 5000 iterations. Finally, several 10 ns MD simulations were carried out with constant temperature constraint at 310, 398, and 498 K. The time step of the MD simulations was 2 fs. The trajectories and coordinates were saved every 1 ps for further analyses.

2.2 *Structural analyses and definition*

The C_α root-mean-square deviations (RMSDs) were calculated from the minimal deviations of the C_α atoms of the trajectories away from the energy-minimised structure. The averaged C_α RMSD value of each residue was also calculated for all trajectories. Secondary structural analysis was carried out using the Kabsch and Sander algorithm [35] incorporated in their DSSP program. The residual β-sheet contents were defined as the ratio of the number of the residues to the total residues in β-sheet of the crystal structure. The distance of the salt–bridge interaction formed by the R3–D59 pair in the wt β2m was also calculated. The solvent accessible surface area (SASA) of the K3 peptide was calculated by the Insight II program as described previously [36]. The distance between the B- and E-strands, defined as the averaged value of the five selected residue pairs, S61–P30, F62–G29, Y63–S28, L64–V27, and L65–Y26, was also calculated.

3. Results

3.1 *Analysis of RMSD*

To investigate the conformational changes of the wt and ΔN6 β2m, various 10-ns MD simulations at 310, 398, and 498 K were conducted in this study. The degree of the structural fluctuations for these two proteins during the MD simulations was simply monitored by the C_α RMSD relative to the corresponding energy-minimised structures and the results are shown in Figure 2(a). It is obvious that the structures of both wt and ΔN6 β2m are very stable at 310 and 398 K, with the C_α RMSD values remaining almost constant around 2–3 Å. It indicates that low simulation temperatures (310 and 398 K) cannot provide sufficient kinetic energy to observe protein unfolding at the simulation time-scale. Therefore, MD simulations at higher temperature (498 K) were required to accelerate the conformational changes of the wt and ΔN6 β2m. Figure 2(a) shows that the C_α RMSD of the ΔN6 β2m is significantly higher than that of the wt β2m at 498 K during most of the simulation courses, suggesting that the ΔN6 β2m is less stable and ready to unfold comparing to the wt β2m.

To further explore the structural flexibility of the wt and ΔN6 β2m at various temperatures, the C_α RMSD per residue of these two proteins were calculated and the results are presented in Figure 2(b). It shows that the residues belonging to the secondary structural elements (β-sheet) in the native state exhibit less structural fluctuation at all simulation temperatures comparing to those located in the other regions. In addition, the largest structural fluctuations appear mainly in the N- and C-terminal regions at 498 K for the ΔN6 β2m. Moreover, the C_α RMSD values of the B- and E-strands of the ΔN6 β2m are significantly higher than those of the wt β2m at 498 K (black arrow in Figure 2(b)).

3.2 *Analysis of secondary structure contents*

The secondary structure contents of the wt and ΔN6 β2m relative to the crystal structure during the 10-ns MD simulations at various temperatures are depicted in Figure 3. It is obvious that the initial secondary structures tend to convert to turns or coils during the MD simulations. Figure 3 also shows that both wt and ΔN6 β2m maintain their structural stability during the entire MD simulation courses at both 310 and 398 K. By contrast, at 498 K, the structural integrities of these two proteins are rapidly disrupted, particularly for the ΔN6 β2m. Furthermore, the result shows that both A- and G-strand of the ΔN6 β2m lose most of their β-sheet contents after around 0.5 ns, indicating that these two strands of the ΔN6 β2m are very sensitive to high simulation temperature.

The averaged β-sheet contents of the wt and ΔN6 β2m are summarised in Table 1. The results show that the averaged β-sheet contents decrease with increasing simulation temperatures. According to Table 1, we found that the stability of the N-terminal A-strand in the ΔN6 β2m is lower than that in the wt β2m at all simulation

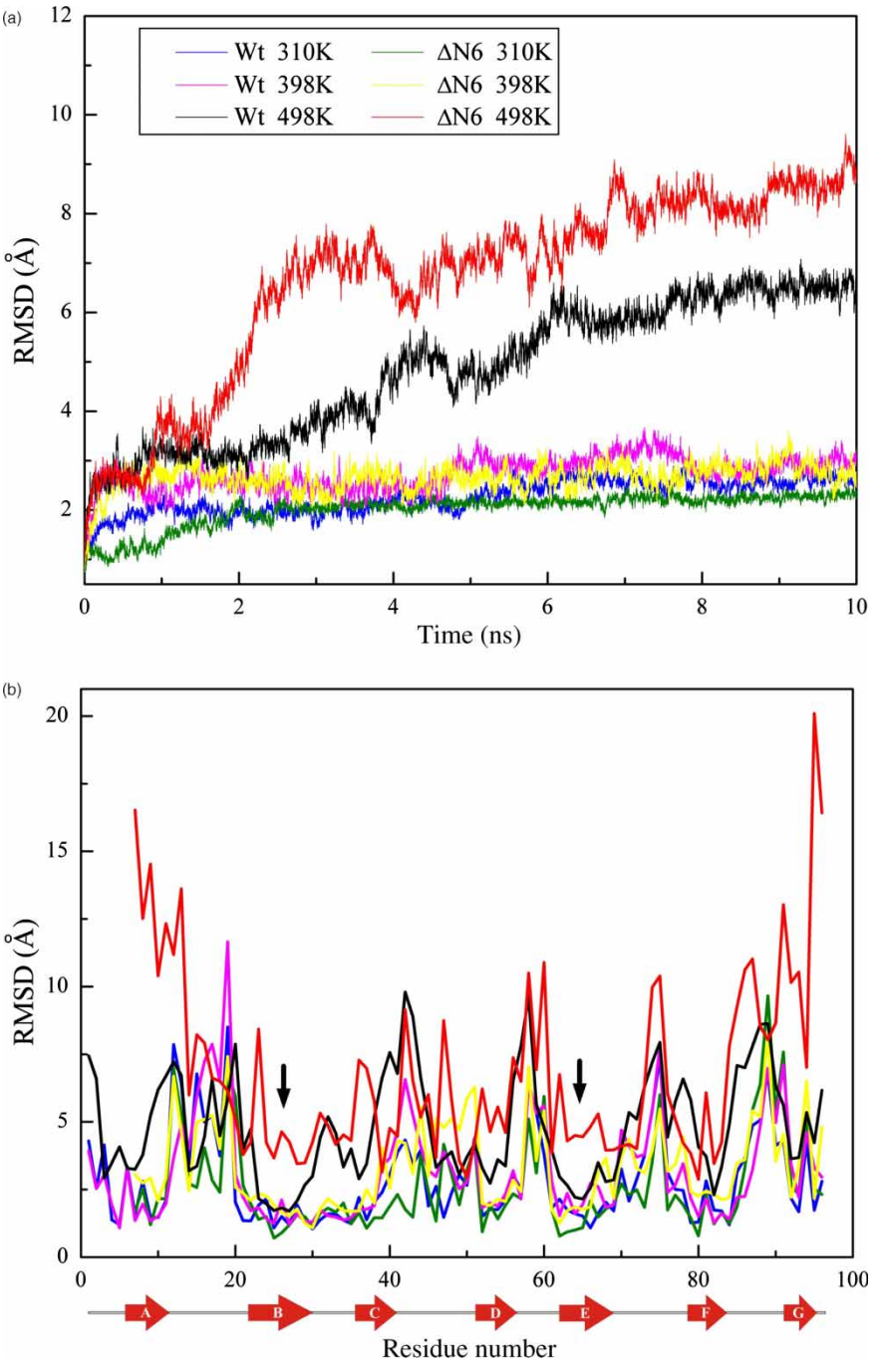

Figure 2. (a) The C_α RMSD and (b) the C_α RMSD per residue of the wt and ΔN6 β2m at various temperatures during the 10-ns MD simulations. The black arrow indicates the large fluctuations of the B- and E-strands for the ΔN6 β2m at 498 K.

temperatures. Additionally, our results further indicate that the B- and E-strands in the ΔN6 β2m are also less stable comparing to those in the wt β2m. The results of secondary structures analysis are consistent with the above analysis of the C_α RMSD per residue shown in Figure 2(b), suggesting that the B- and E-strands are less structurally stable in the ΔN6 β2m than in the wt β2m.

3.3 Analysis of the distances between residues R3 and D59

The structural difference between the ΔN6 and wt β2m is that the ΔN6 β2m lacks the N-terminal six residues. Due to the deletion of the N-terminal six residues, the ΔN6 β2m loses a salt–bridge interaction between residues R3 and D59. To elucidate the role of this salt–bridge

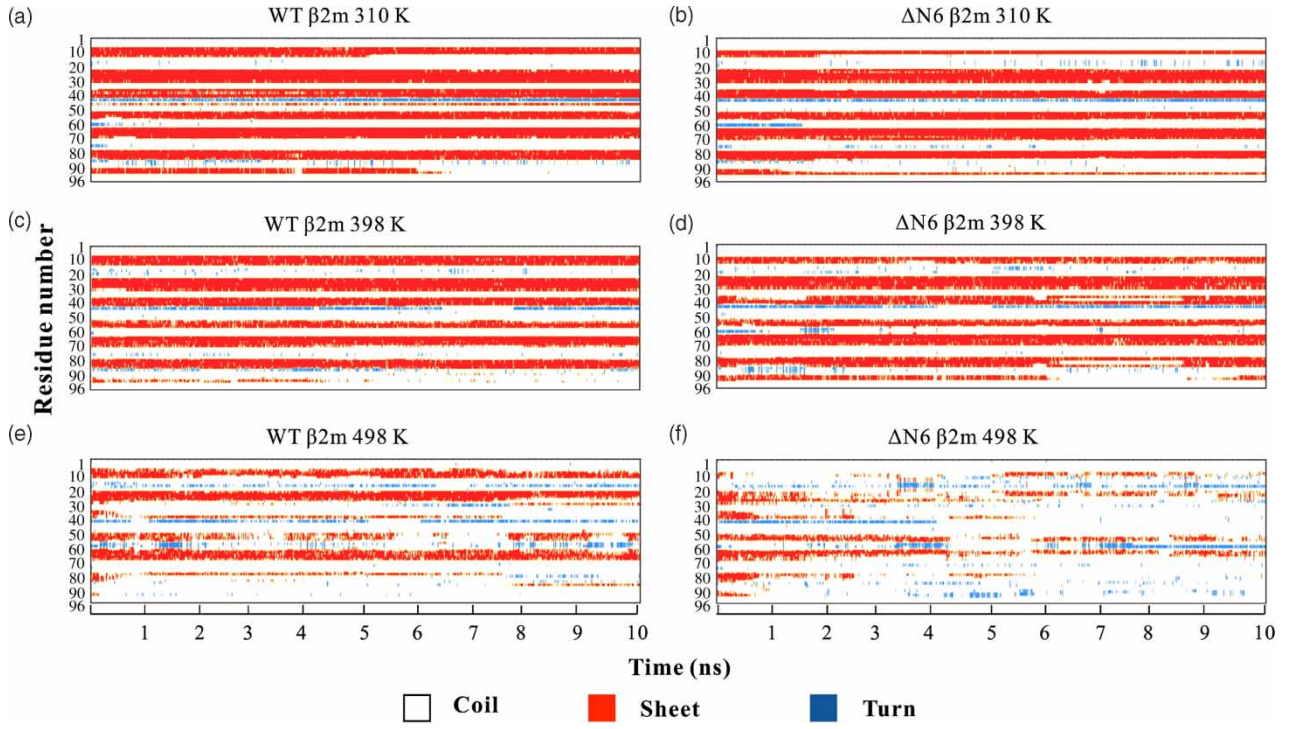

Figure 3. The secondary structures contents of (a) the wt β2m at 310 K; (b) the ΔN6 β2m at 310 K; (c) the wt β2m at 398 K; (d) the ΔN6 β2m at 398 K; (e) the wt β2m at 498 K; and (f) the ΔN6 β2m at 498 K. The β-sheet, turn, and coil estimated according to DSSP (Kabsch and Sander, 1983) are shown in red, blue, and white, respectively.

interaction in maintaining the structural stability of β2m, the distances between residues R3 and D59 in the wt β2m were calculated and the results are shown in Figure 4. It is obvious that the distances between residues R3 and D59 reach to the equivalent value around 6–8 Å after 100 ps at all simulation temperatures from the initial value of 14 Å, indicating that this strong salt–bridge interaction contributes to maintaining the structural stability of the N-terminal strand of the wt β2m. Our results are in good agreement with the results from the previous mutational analysis, in which the R3A mutant reduces the unfolding free energy compared with wt β2m, suggesting that the residue R3 play an important role in maintaining the globular structure of β2m from destabilisation [37]. The importance of the salt–bridge interaction between Asp–Arg on protein stability is further supported by a recent study [38], in which the Asp–Arg interaction has been identified as a fork–fork salt bridge with a interaction distance of nearly 6 Å. This type of interactions, such as Asp–Arg and Glu–Arg fork–fork salt bridges, are more favourable in the thermostable proteins, with a nice energy progression from the psychrostable to the hyperthermostable proteins [38].

3.4 Analysis of the SASA of the K3 peptide

Previous study has found that the 22-residue peptide fragment of Ser20–Lys41 (B- and C-strands), known as the K3 peptide, retains the potential to form typical

Table 1. Averaged β-sheet contents of the wt and ΔN6 β2m at different temperatures during the entire simulation courses.

		Averaged β-sheet contents (%)							
	Protein temperature (K)	A	B	C	D	E	F	G	Total
Wt	310	83.3	98.1	89.3	93.2	97.7	94.5	56.9	90.0
ΔN6	310	66.6	94.4	97.5	91.2	98.3	97.9	51.8	88.1
Wt	398	94.8	94.8	88.3	76.9	89.8	88.7	18.3	83.3
ΔN6	398	83.0	92.9	78.4	72.6	94.2	82.6	44.2	81.4
Wt	498	65.0	68.9	18.2	43.3	75.3	18.7	0.51	47.0
ΔN6	498	19.3	28.0	14.1	41.6	41.2	14.3	3.65	28.2

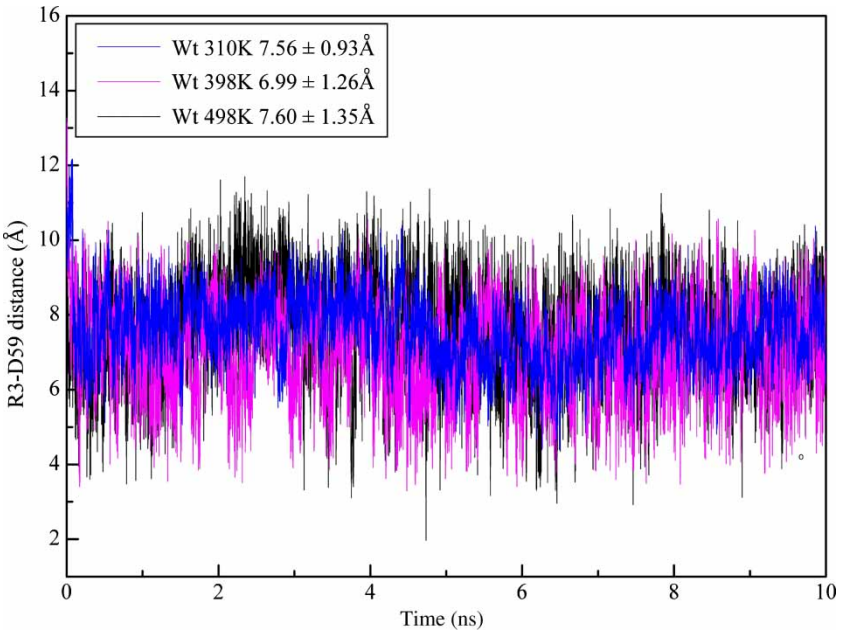

Figure 4. The distances of the salt–bridge interaction between the R3–D59 pair in the wt β2m at various temperatures during the 10-ns MD simulations. The salt–bridge interaction is simply measured by the distances between the nitrogen atom on the side chain of R3 residue and the oxygen atom on the side chain of D59 residue.

amyloid fibrils, suggesting that this short segment includes a minimal region for the formation of amyloid fibrils of β2m [16]. In order to investigate the role of the K3 peptide in the conformational changes of the wt and ΔN6 β2m, the SASAs of the K3 peptide was calculated at different temperatures and the results were depicted in Figure 5. The results show that the SASA values of the K3 peptide for both wt and ΔN6 β2m are very stable during the entire simulation courses at both 310 and 398 K. By contrast, the solvent exposure of the K3 peptide increased dramatically at 498 K, particularly for the ΔN6 β2m. These results indicate that the K3 peptide of the ΔN6 β2m exhibits greater structural fluctuation compared to that of the wt β2m at 498 K.

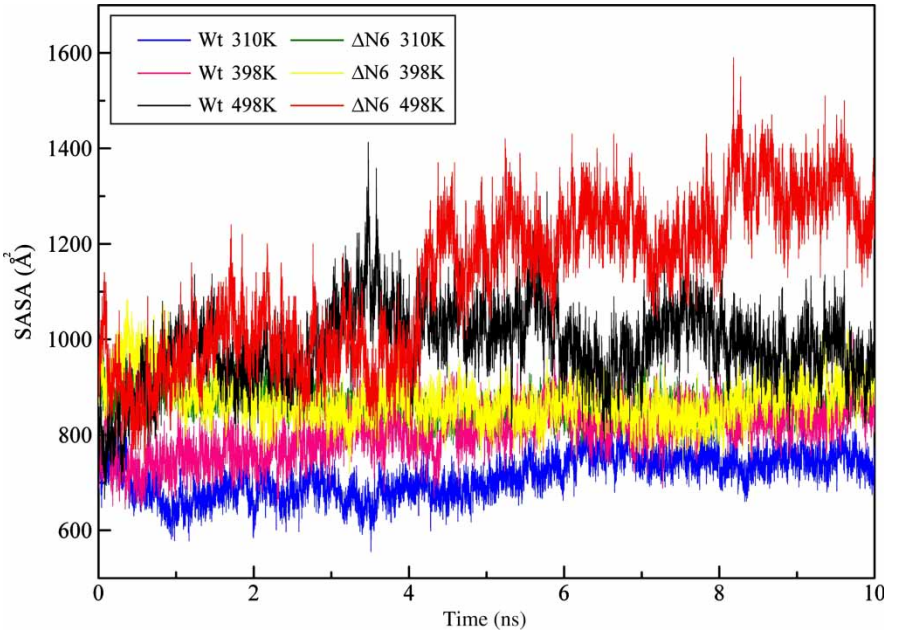

Figure 5. The SASA of the K3 peptide of the wt and ΔN6 β2m in water at various temperatures during the 10-ns MD simulations.

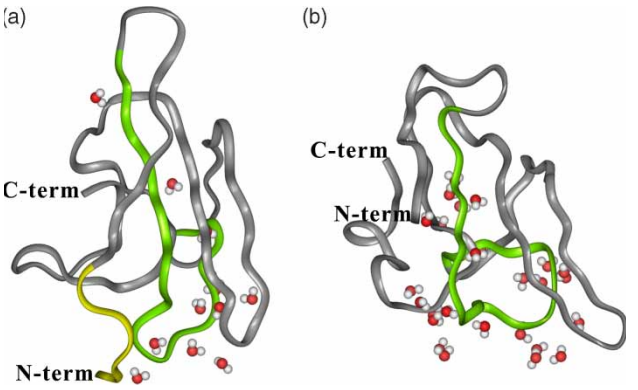

Figure 6. Solvation of the K3 peptide of the (A) wt and (B) ΔN6 β2m at 498 K. The truncation of the N-terminal six residues for the ΔN6 β2m, yellow; The interfacial water molecules at a distance of < 2.4 Å from the K3 peptide are also shown.

Figure 6 shows the snapshots of the solvation of the K3 peptide for the wt and ΔN6 β2m taken from the simulations at 498 K. It is obvious that the increased solvent exposure of the K3 peptide for the ΔN6 β2m inevitably allows water molecules to directly contact with the interior region of the K3 peptide. Moreover, some water molecules were found to penetrate into the interior region between B- and E-strands in the ΔN6 β2m, indicating that the exposure and mobility of the K3 peptide is possibly associated with the disruption of the B- and E-strands.

3.5 Analysis of the SASA against the C_α distances between the B- and E-strands

To further investigate the effects of the solvent exposure and mobility of the K3 peptide on the disruption of the B- and E-strands, two plots of SASA of the K3 peptide against the distances between the B- and E-strands are presented in Figure 7. It shows that the trajectories of the wt and ΔN6 β2m assemble to clusters at 310 and 398 K, indicating that the SASA values of the K3 peptide and the distances between the B- and E-strands remain approximately constants during the simulation course. By contrast, our results show an L-shaped profile for the ΔN6 β2m at 498 K, suggesting that the K3 peptide in the ΔN6 β2m exposes to solvent significantly, followed by the elongation of the B- and E-strands.

Figure 8 shows the averaged structures of the B- and E-strands in the wt and ΔN6 β2m during the MD simulations at 498 K. In the wt β2m, it is clear that the distances between the B- and E-strands increase slightly during the simulation course. By contrast, the distances between the B- and E-strands increase rapidly in the ΔN6 β2m, leading to accelerating protein unfolding more effectively than in the wt β2m.

4. Discussion

4.1 The ΔN6 β2m exhibits lower structural stability comparing to the wt β2m

Previously, analysis of *ex vivo* fibrils from DRA patients has shown that around 30% of the β2m molecules display truncations in the N-terminal strand, suggesting that these strands are not involved in the core of the assembled fibril [6,18]. Limited proteolysis has shown that a β2m lacking the N-terminal six residues (ΔN6 β2m) exhibit a higher tendency to form amyloids at neutral pH [18–20]. Myers et al. [21] have shown that the ΔN6 β2m forms low yields of amyloid-like fibrils at pH 7 in the absence of seeds, suggesting that this species could initiate fibrillogenesis *in vivo*. Piazza et al. [22] suggested that the addition of tiny amounts of the ΔN6 β2m to the wt β2m rapidly leads to the formation of large aggregates, demonstrating a seeding capacity of this species in promoting β2m aggregation. Additionally, several studies have suggested that the unfolding of the protein into a partially unfolded conformation is required for the formation of aggregates and fibrils [6,39]. Altogether, these evidences imply that the ΔN6 β2m exhibit higher tendency to form amyloid fibrils due to its lower structural stability compared with the wt β2m.

The results of the current MD simulations, in agreement with the above viewpoints, show that the C_α RMSD value of the ΔN6 β2m is higher than that of the wt β2m at 498 K, indicating that the entire structure of the ΔN6 β2m is more flexible than that of the wt β2m at high simulation temperature (Figure 2(a)). Moreover, the analysis of the secondary structure contents also indicate that the β-sheet stability of the ΔN6 β2m is lower than that of the wt β2m (Figure 3 and Table 1), particularly at 498 K.

4.2 The increased exposure of K3 peptide results in the elongation between B- and E-strands

Previous study has shown that the K3 peptide (Ser21–Lys41) constitutes the essential region of the β2m-related amyloid fibril formation [16]. This minimal sequence provides various pieces of information useful for addressing amyloid fibril formation. It is likely that the K3 peptide includes the initiation site for the amyloid fibril formation of the full-length β2m molecule. Moreover, it may constitute the core of the consequent amyloid fibrils. Previous study has shown that an optimum for the K3 fibril formation exists at neutral pH, suggesting that, once the rigid native β2m is unfolded and additional factors triggering the nucleation process are provided, the full-length β2m discloses an intrinsic potential to form amyloid fibrils at neutral pH [17].

In the present study, the analysis of SASA of the K3 peptide was conducted to investigate the role of the K3 peptide in the unfolding process of the wt and ΔN6 β2m.

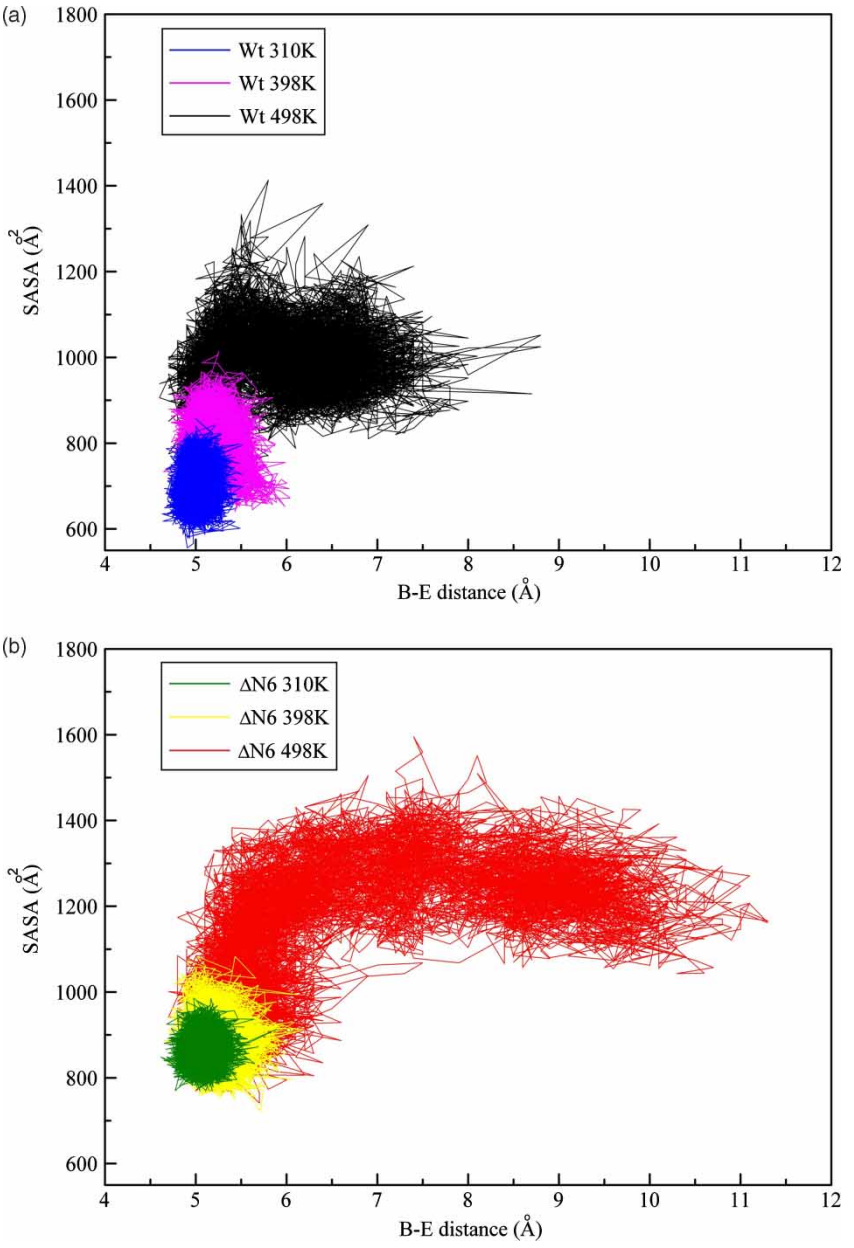

Figure 7. The relationships between the SASA of the K3 peptide and the distance between the B- and E-strands of the (a) wt and (b) ΔN6 β2m at various temperatures during the 10-ns MD simulations.

Our results show that the K3 peptide of the ΔN6 β2m exposed to solvent more significantly comparing to that of the wt β2m, particularly at 498 K (Figure 5), suggesting that the K3 peptide may be a potential nucleation site for the amyloidogenic process of the ΔN6 β2m. Furthermore, our results also indicate that the increased exposure of the K3 peptide of the ΔN6 β2m results in the elongation between the B- and E-strands (Figures 7 and 8). These observations are in good agreement with the results from the previous study, where the main effect of the removal of the N-terminal six residues in the wt β2m was found to increase the separation between the B- and E-strands [40].

4.3 The importance of the N-terminal six residues and salt–bridge interaction between R3-D59

It has been suggested that the A- and G-strands are the most unstable segments of β2m and are involved in the amyloidogenic process. The A- and G-strands were found to be the most sensitive strands to urea denaturation [41]. A hydrogen–deuterium exchange study has revealed that the A- and G-strands do not participate in the amyloid fibril [42]. Furthermore, the A- and G-strands were found to be protected in the globular state and unprotected in the fibrillar state, using limited proteolysis [43]. The involvement of the A- and G-strands in amyloidogenesis was further

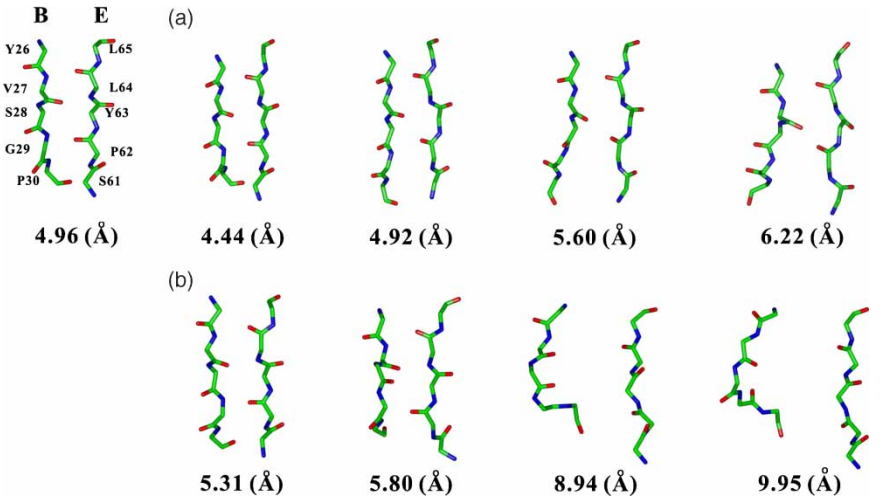

Figure 8. Snapshots of the averaged structures (per 2.5 ns) of the (a) wt and (b) ΔN6 β2m at 498 K. The averaged distances between the B- and E-strands are shown below theses averaged structures.

demonstrated in the observation that mutations of the residues in these strands accelerate amyloidogenesis [44]. Moreover, it has been shown that partially unfolded β2m formed by acidification to pH 3.6 displays significant destabilisation of both the N and C-terminal strands [41]. These data all demonstrated that the perturbation of the N- and C-terminal edge strands is an important feature in the generation of assembly-competent states of β2m.

The results of the present simulations, in agreement with the above experimental findings, show that both the N-terminal A-strand and C-terminal G-strand exhibit lower structural stability, particularly for the ΔN6 β2m at 498 K (Figure 2(b) and Table 1). Furthermore, our results also show that the deletion of the N-terminal six residues leads to the increased exposure of the K3 peptide significantly (Figure 5), which allows water molecules to destabilise the interior region of the K3 peptide (Figure 6), leading to greater mobility and the elongation between the B- and E-strands (Figures 7 and 8). These evidences all suggest that the N-terminal six residues play an important role in protecting the globular structure of β2m from destabilisation, which is also consistent with the results from the previous study [43].

A salt–bridge interaction between residues R3 and D59 was found in the wt β2m in this study (Figure 4). Our simulation results show that the distances between residues R3 and D59 reach to the value around 6–8 Å from the initial value of 14 Å at different temperatures, indicating that this strong salt–bridge interaction contributes significantly to the structural stability of N-terminal A-strand in the wt β2m. It further plays a role to protect the global structure of the native protein from partially unfolding. Our results are consistent with the previous mutational and free energy analyses showing that the R3A mutant is less stable than wt β2m [37]. In summary, the lack of the N-terminal six residues and the loss of the salt–bridge interaction between R3 and D59 in the ΔN6 β2m result in the destabilisation of its native structure, which further accelerates the conformational changes leading to the formation of amyloid fibrils at neutral pH.

4.4 Insights into the morphologies of amyloid fibrils of the ΔN6 β2m from MD simulations

Figure 9 summarises the amyloid morphologies and the related unfolding intermediates of the wt and ΔN6 β2m reported previously. Two distinct fibril morphologies of the wt β2m under various low pH conditions have been reported. One is the short curved fibrils at pH 3.5 and the other one is the long and straight fibrils at pH 2.5 [11–13]. Smith et al. [11] have pointed out that these two distinct morphologies are specifically related to the two unfolding intermediates, I_1 and I_2, respectively. Some evidences have suggested that the curved fibrils are derived from the native-like I_1, which is the dominant conformation at pH 4 [45]; whereas the linear fibrils form slowly from the more disordered I_2, which is the dominant conformation at pH 1.6 [45]. Interestingly, *ex vivo* fibrils exhibit predominantly curved morphology [46,47] and they are presumably formed from I_1 or something similar. Recently, Armen and Daggett [14] have proposed that I_1 forms fibrils primarily via the stable B- and E-strands, which exhibit the largest difference in the numbers of contacts between I_1 and I_2, as well as the greatest stability against urea denaturation at pH 3.5 [41].

The results of this study show that the B- and E-strands of the ΔN6 β2m are more dynamic and less stable comparing to those of the wt β2m, particularly at 498 K, which are consistent with the findings from the previous study [40]. However, the domain-swapped model of the wt

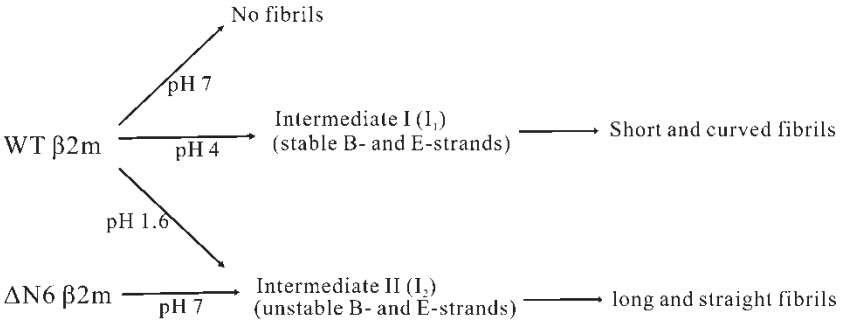

Figure 9. Schematic representations of the amyloid morphologies and their related unfolding intermediates of the wt and ΔN6 β2m.

β2m proposed by Chen and Dokholyan [15] reveals that B- and E-strands are very stable, suggesting the difference in molecular mechanisms underlying the aggregation of the wt and ΔN6 β2m. Moreover, the ΔN6 β2m may be difficult to aggregate through domain swapping due to the removal of the N-terminal six residues. Here, our results indicate that the increased exposure of the K3 peptide of the ΔN6 β2m leads to the elongation between the B- and E-strands (Figures 7 and 8), which is one of the important structural features of I_2 proposed by Armen and Daggett [14]. The previous findings and the present simulation results led us propose that the amyloidogenic intermediate of the ΔN6 β2m at neutral pH may be similar to I_2 due to the elongation between the B- and E-strands. Therefore, we suggest that the fibril morphologies of the ΔN6 β2m at neutral pH is similar to that of the wt β2m at low pH conditions (1.5–3), which is also in good agreement with the previous experimental results showing that fibril morphologies of the ΔN6 β2m at pH 7 and wt β2m at pH ∼2.5 are long and straight [11–13].

5. Conclusions

In this study, various MD simulations were conducted to investigate the conformational changes of the wt and ΔN6 β2m at various temperatures (310, 398, and 498 K) at pH 7. Present analyses indicate that the loss of the structural stability of the ΔN6 β2m may accelerate the conformational changes, leading to the formation of amyloid fibrils at neutral pH more readily comparing to the wt β2m. There is always an open question about what is the role of N-terminal six residues in the structural stability of β2m. Our simulation results indicate that the removal of the N-terminal six residues and the loss of the salt–bridge interaction between residues R3 and D59 lead to the increased exposure of the K3 peptide (Figure 5), which allows water molecules to destabilise the interior region of the K3 peptide (Figure 6), leading to the greater mobility and the elongation between the B- and E-strands (Figures 7 and 8). We further found that the amyloidogenic intermediate of the ΔN6 β2m at neutral pH may be similar to I_2 due to the elongation between the B- and E-strands. Therefore, we propose that the fibril morphology of the ΔN6 β2m formed at neutral pH may be similar to that of the wt β2m formed at low pH (1.5–3) conditions. Furthermore, our results also demonstrate that the solvent exposure of the K3 peptide of the ΔN6 β2m increases significantly, suggesting that the K3 peptide may be a potential initiation site for the amyloid formation.

Acknowledgement

The authors gratefully acknowledge the financial support (Project number: NSC 96-2221-E-027-045-MY3) from the National Science Council of Taiwan.

References

[1] F.E. Cohen and J.W. Kelly, *Therapeutic approaches to protein-misfolding diseases*, Nature 426 (2003), pp. 905–909.
[2] C.M. Dobson, *Protein folding and misfolding*, Nature 426 (2003), pp. 884–890.
[3] F. Chiti and C.M. Dobson, *Protein misfolding, functional amyloid, and human disease*, Ann. Rev. Biochem. 75 (2006), pp. 333–366.
[4] D. Thirumalai, D.K. Klimov, and R.I. Dima, *Emerging ideas on the molecular basis of protein and peptide aggregation*, Curr. Opin. Struct. Biol. 13 (2003), pp. 146–159.
[5] K.M. Koch, *Dialysis-related amyloidosis*, Kidney Int. 41 (1992), pp. 1416–1429.
[6] J. Floege and M. Ketteler, *Beta2-microglobulinderived amyloidosis: an update*, Kidney Int. 59 (2001), pp. 164–171.
[7] T. Miyata, M. Jadoul, K. Kurokawa, and C. van Ypersele de Strihou, *Beta2-microglobulin in renal disease*, J. Am. Soc. Nephrol. 9 (1998), pp. 1723–1735.
[8] N. Homma, F. Gejyo, M. Isemura, and M. Arakawa, *Collagen-binding affinity of beta2-microglobulin, a preprotein of hemodialysis-associated amyloidosis*, Nephron 53 (1989), pp. 37–40.
[9] M.A. Saper, P.J. Bjorkman, and D.C. Wiley, *Refined structure of the human histocompatibility antigen HLA-A2 at 2.6 Å resolution*, J. Mol. Biol. 219 (1991), pp. 277–319.
[10] C.H. Trinh, D.P. Smith, A.P. Kalverda, S.E. Phillips, and S.E. Radford, *Crystal structure of monomeric human beta2-microglobulin reveals clues to its amyloidogenic properties*, Proc. Natl Acad. Sci. USA 99 (2002), pp. 9771–9776.
[11] D.P. Smith, S. Jones, L.C. Serpell, M. Sunde, and S.E. Radford, *A systematic investigation into the effect of protein destabilisation on beta2-microglobulin amyloid formation*, J. Mol. Biol. 330 (2003), pp. 943–954.
[12] W.S. Gosal, I.J. Morten, E.W. Hewitt, D.A. Smith, N.H. Thomson, and S.E. Radford, *Competing pathways determine fibril morphology*

in the self-assembly of beta2-microglobulin into amyloid, J. Mol. Biol. 351 (2005), pp. 850–864.
[13] S.L. Myers, S. Jones, T.R. Jahn, I.J. Morten, G.A. Tennent, E.W. Hewitt, and S.E. Radford, *A systematic study of the effect of physiological factors on beta2-microglobulin amyloid formation at neutral pH*, Biochemistry 45 (2006), pp. 2311–2321.
[14] R.S. Armen and V. Daggett, *Characterization of two distinct beta2-microglobulin unfolding intermediates that may lead to amyloid fibrils of different morphology*, Biochemistry 44 (2005), pp. 16098–16107.
[15] Y. Chen and N.V. Dokholyan, *A single disulfide bond differentiates aggregation pathways of beta2-microglobulin*, J. Mol. Biol. 354 (2005), pp. 473–482.
[16] G.V. Kozhukh, Y. Hagihara, T. Kawakami, K. Hasegawa, H. Naiki, and Y. Goto, *Investigation of a peptide responsible for amyloid fibril formation of beta2-microglobulin by achromobacter protease I*, J. Biol. Chem. 277 (2002), pp. 1310–1315.
[17] Y. Ohhashi, K. Hasegawa, H. Naiki, and Y. Goto, *Optimum amyloid fibril formation of a peptide fragment suggests the amyloidogenic preference of beta2-microglobulin under physiological conditions*, J. Biol. Chem. 279 (2004), pp. 10814–10821.
[18] V. Bellotti, M. Stoppini, P. Mangione, M. Sunde, C. Robinson, L. Asti, D. Brancaccio, and G. Ferri, *Beta2-microglobulin can be refolded into a native state from* ex vivo *amyloid fibrils*, Eur. J. Biochem. 258 (1998), pp. 61–67.
[19] G. Esposito, R. Michelutti, G. Verdone, P. Viglino, H. Hernandez, C.V. Robinson, A. Amoresano, F. Dal Piaz, M. Monti, P. Pucci, et al., *Removal of the N-terminal hexapeptide from human beta2-microglobulin facilitates protein aggregation and fibril formation*, Protein Sci. 9 (2000), pp. 831–845.
[20] V. Bellotti, M. Gallieni, S. Giorgetti, and D. Brancaccio, *Dynamic of beta2-microglobulin fibril formation and reabsorption: the role of proteolysis*, Semin. Dial. 14 (2001), pp. 117–122.
[21] S.L. Myers, N.H. Thomson, S.E. Radford, and A.E. Ashcroft, *Investigating the structural properties of amyloid-like fibrils formed* in vitro *from beta2-microglobulin using limited proteolysis and electrospray ionization mass spectrometry*, Rapid Commun. Mass Spectrom. 20 (2006), pp. 1628–1636.
[22] R. Piazza, M. Pierno, S. Iacopini, P. Mangione, G. Esposito, and V. Bellotti, *Micro-heterogeneity and aggregation in beta2-microglobulin solutions: effects of temperature, pH, and conformational variant addition*, Eur. Biophys. J. 35 (2006), pp. 439–445.
[23] H.-L. Liu, Y.-C. Wu, J.-H. Zhao, H.-W. Fang, and Y. Ho, *Structural analysis of human lysozyme using molecular dynamics simulations*, J. Biomol. Struct. Dynam. 24 (2006), pp. 229–238.
[24] H.-L. Liu, Y.-C. Wu, J.-H. Zhao, Y.-F. Liu, C.-H. Huang, H.-W. Fang, and Y. Ho, *Insights into the conformational changes of several human lysozyme variants associated with hereditary systemic amyloidosis*, Biotechnol. Prog. 23 (2007), pp. 246–254.
[25] Y.-M. Lin, H.-L. Liu, J.-H. Zhao, C.-H. Huang, H.-W. Fang Y.H., and W.-Y. Chen, *Molecular dynamics simulations to investigate the domain swapping mechanism of human cystatin C*, Biotechnol. Prog. 23 (2007), pp. 577–584.
[26] H.-L. Liu, Y.-M. Lin, J.-H. Zhao, M.-C. Hsieh, H.-Y. Lin, C.-H. Huang, H.-W. Fang, Y. Ho, and W.-Y. Chen, *Molecular dynamics simulations of human cystatin C and its L68Q varient to investigate the domain swapping mechanism*, J. Biomol. Struct. Dynam. 25 (2007), pp. 135–144.
[27] H.-L. Liu, C.-T. Yang, J.-H. Zhao, C.-H. Huang, H.-Y. Lin, H.-W. Fang, Y. Ho, and W.-B. Tsai, *Molecular dynamics simulations to investigate the effects of zinc ions on the structural stability of the c-Cbl RING domain*, Biotechnol. Prog. 23 (2007), pp. 1231–1238.
[28] J.-H. Zhao, C.-T. Yang, J.-W. Wu, W.-B. Tsai, H.-Y. Lin, H.-W. Fang, Y. Ho, and H.-L. Liu, *RING domains with E3 ligase functions reveal distinct structural features: a molecular dynamics simulation study*, J. Biomol. Struct. Dynam. 26 (2008), pp. 65–74.
[29] D. Trzesniak, R.D. Lins, and W.F. van Gunsteren, *A protein under pressure: molecular dynamics simulation of the arc repressor*, Proteins 65 (2006), pp. 136–144.
[30] J.-H. Zhao and H.-L. Liu, *The effects of various alcohols on the structural stability of melittin, TH-10Aox, and Tc1 by molecular dynamics simulations*, Chem. Phys. Lett. 420 (2006), pp. 235–240.
[31] R. Day, B. Bennion, S. Ham, and V. Daggett, *Increasing temperature accelerates protein unfolding without changing the pathway of unfolding*, J. Mol. Biol. 322 (2002), pp. 189–203.
[32] M.J. Hwang, X. Ni, X. Waldman, C.S. Ewig, and A.T. Hagler, *Derivation of class II force fields. VI. Carbohydrate compounds and anomeric effects*, Biopolymers 45 (1998), pp. 435–468.
[33] M.P. Allen and D.J. Tildesley, *Computer Simulations of Liquids*, Clarendon Press, Oxford, 1987.
[34] G.S. Kell, *Precise representation of volume properties of water at one atmosphere*, J. Chem. Eng. Data 12 (1967), pp. 66–69.
[35] W. Kabsch and C. Sander, *Dictionary of protein secondary structure: pattern recognition of hydrogen-bonded and geometrical features*, Biopolymers 22 (1983), pp. 2577–2637.
[36] G. Nimrod, F. Glaser, D. Steinberg, N. Ben-Tal, and T. Pupko, In silico *identification of functional regions in proteins*, Bioinformatics 1 (2005), pp. 328–337.
[37] A. Corazza, F. Pettirossi, P. Viglino, G. Verdone, J. Garcia, P. Dumy, S. Giorgetti, P. Mangione, S. Raimondi, M. Stoppini, et al., *Properties of some variants of human beta2-microglobulin and amyloidogenesis*, J. Biol. Chem. 279 (2004), pp. 9176–9189.
[38] B. Folch, M. Rooman, and Y. Dehouck, *Thermostability of salt bridges versus hydrophobic interactions in proteins probed by statistical potentials*, J. Chem. Inf. Model. 48 (2008), pp. 119–127.
[39] F. Chiti, E. De Lorenzi, S. Grossi, P. Mangione, S. Giorgetti, G. Caccialanza, C.M. Dobson, G. Merlini, G. Ramponi, and V. Bellotti, *A partially structured species of beta2-microglobulin is significantly populated under physiological conditions and involved in fibrillogenesis*, J. Biol. Chem. 276 (2001), pp. 46714–46721.
[40] B. Ma and R. Nussinov, *Molecular dynamics simulations of the unfolding of beta2-microglobulin and its variants*, Protein Eng. 11 (2003), pp. 561–575.
[41] V.J. McParland, A.P. Kalverda, S.W. Homans, and S.E. Radford, *Structural properties of an amyloid precursor of beta2-microglobulin*, Nat. Struct. Biol. 9 (2002), pp. 326–331.
[42] M. Hoshino, H. Katou, Y. Hagihama, K. Hasegawa, H. Naiki, and Y. Goto, *Mapping of the beta2-microglobulin core by H/D exchange monitored by NMR*, Nat. Struct. Biol. 9 (2002), pp. 323–325.
[43] M. Monti, S. Principe, S. Giorgetti, P. Mangione, G. Merlini, A. Clark, V. Bellotti, A. Amoresano, and P. Pucci, *Topological investigation of amyloid fibrils obtained from beta2-microglobulin*, Protein Sci. 11 (2002), pp. 2362–2369.
[44] S. Jones, D.P. Smith, and S.E. Radford, *Role of the N and C-terminal strands of beta2-microglobulin in amyloid formation at neutral pH*, J. Mol. Biol. 330 (2003), pp. 935–941.
[45] V.J. McParland, N.M. Kad, A.P. Kalverda, A. Brown, P. Kirwin-Jones, M.G. Hunter, M. Sunde, and S.E. Radford, *Partially unfolded states of beta2-microglobulin and amyloid formation* in vitro, Biochemistry 39 (2000), pp. 8735–8746.
[46] S. Nishi, S. Ogino, Y. Maruyama, N. Honma, F. Gejyo, T. Morita, and M. Arakawa, *Electron-microscopic and immunohistochemical study of beta2-microglobulin-related amyloidosis*, Nephron 56 (1990), pp. 357–363.
[47] S. Inoue, M. Kuroiwa, K. Ohashi, M. Hara, and R. Kisilevsky, *Ultrastructural organization of hemodialysis-associated beta2-microglobulin amyloid fibrils*, Kidney Int. 52 (1997), pp. 1543–1549.